BNL-212012-2019-TECH

CBETA/046

The effects of a finite beam pipe on resistive wall instabilities

J. Christie, S. Peggs

August 2019

Collider Accelerator Department

Brookhaven National Laboratory

U.S. Department of Energy

USDOE Office of Science (SC), Nuclear Physics (NP) (SC-26)

DISCLAIMER

The Effects of a Finite Beam Pipe on Resistive Wall Instabilities

J. Christie, Oxford University
jonathan.christie@trinity.ox.ac.uk

August 6, 2019

Abstract

The effect of resistive wall instabilities on beam break-up is investigated for beam pipes with finite and infinite thickness walls. Analytic solutions for the electric field along the beam axis are determined for both finite and infinite thickness walls using complex analysis. The longitudinal and transverse impedances are also determined; variations from the infinite wall case are observed when the wall thickness is of the order of the skin depth of the beam pipe material.

1 Introduction

Resistive wall instabilities occur when charged particles travel through a beam pipe made out of a metal with a finite conductivity, and can lead to beam break-up in linear accelerators if not accounted for due to its long-range nature [1].

Consider a beam of evenly spaced bunches of charged particles (called macroparticles) that are slightly offset from the central axis of the beam pipe. The beam propagates through an infinitely long linear accelerator at approximately the speed of light. As it does so, the electromagnetic field of the first macroparticle propagates to the beam pipe walls.

If the walls were perfectly conducting, the electromagnetic field would terminate at the surface of the beam pipe wall and there would be no instability.

However, since the walls have some large but finite conductivity, the electromagnetic field from the macroparticle penetrates slightly into the beam pipe wall itself. This leads to a residual electromagnetic field being present within the walls themselves in order to satisfy the necessary boundary conditions.

As a result, the next macroparticle in the beam has its trajectory affected by the residual electromagnetic field, whilst also contributing to the total residual electromagnetic field, resulting in larger and larger deviations in macroparticle trajectories and, eventually, beam break-up.

This instability can be demonstrated using a simple model [2]. A beam of $n_m \approx 10^6$ macroparticles separated by $z \approx 1$ mm, each containing $n_b \approx 10^9$ electrons, initially propagates near the centre of a perfectly conducting, infinitely long pipe with infinitely thick walls. The beam has an initial offset $x_j \approx 1$ μm from the central axis of the beam pipe. The beam then encounters a section of length $L \approx 1000$ m with finite conductivity $\sigma \approx 2 \times 10^6$ $\Omega^{-1}\mathrm{m}^{-1}$. The resulting net angular kick to macroparticle i after passing through the resistive section in SI units is thus given by

$$\Delta x_i' = \frac{n_b e^2}{m_e c^2 \gamma} \frac{1}{n_m} \sum_{j=1}^{n_m} W_1(z_j - z_i) x_j \ , \tag{1}$$

where $\gamma \approx 100$ is the gamma factor of the 50 MeV electrons, e is the electronic charge, m_e is the rest mass of the electron, and c is the speed of light. $W_1(z_j - z_i)$, the transverse wake field, describes how the beam pipe responds to the dipole moment of the particle beam. At long distances behind the bunch, the transverse wake field in SI units is given by

$$W_1(z) \approx \frac{2L}{\pi b^3} \sqrt{\frac{c}{4\pi\epsilon_0\sigma}} \frac{1}{|z|^{\frac{1}{2}}} \ , \tag{2}$$

where ϵ_0 is the permittivity of free space, and $b \approx 5$ cm is the radius of the beam pipe.

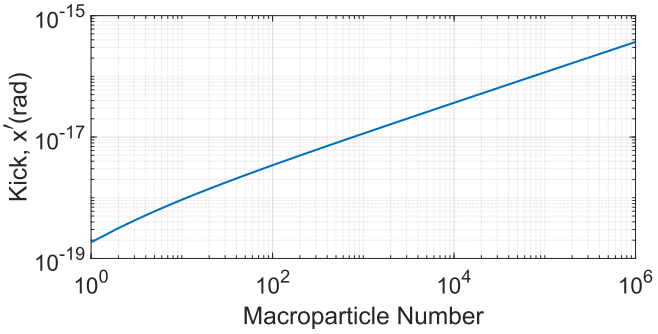

Figure 1: Net transverse angular kick received by each bunch

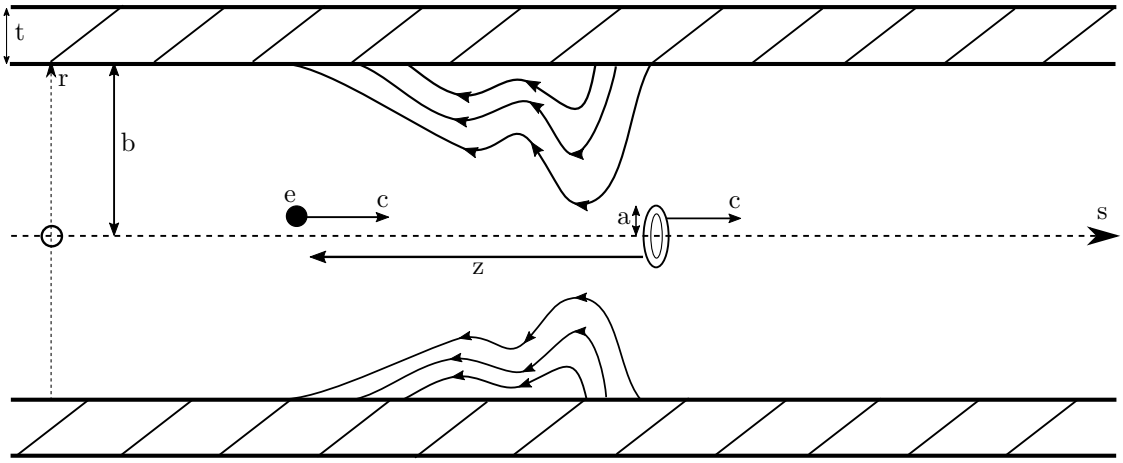

Figure 2: Beam pipe layout [1]

Because the macroparticles are moving at approximately the speed of light, causality requires that the wake field generated by a given macroparticle is zero in front of that particle. As a result, a given macroparticle i can only be affected by the wake generated by the macroparticles in front of it.

Using this form of the long-range wake field, it is relatively straightforward to simulate the above model and determine how the net angular kick received by each macroparticle varies with macroparticle number, as shown in Figure 1.

From the plot, it is clear that, at large bunch numbers, the net angular kick received by each macroparticle is proportional to the square root of the macroparticle number, and hence proportional to the square root of distance from the first macroparticle. As a result, such instabilities continue to grow as more macroparticles pass, until beam break-up occurs.

However, when deriving the form of W_1 in Equation 2, it was assumed that the pipe walls were infinitely thick. Whilst this is usually a good approximation for short-range wake effects, it is not necessarily good for long-range effects, especially if the pipe walls have a thickness on the order of the skin depth of the metal at frequencies of interest.

Assuming that the pipe walls have some finite thickness t, different boundary conditions apply. This leads to different expressions for the wake field and its Fourier transform, known as the impedance.

This note investigates the effects that wall thickness has on the long-range wake fields and on the low-frequency impedances, potentially leading to a feasible system with reduced resistive wall instabilities and hence a more stable beam.

2 Resistive Wall Wake Fields

2.1 Solving Maxwell's Equations

The first step towards finding the electromagnetic fields and wake fields is to solve Maxwell's equations in cylindrical coordinates. Given that the initial distribution of the charge creating the wake field is unknown, we can write charge density ρ and current density $\vec{j}$ in terms of their multipole moments,

$$\begin{aligned} \rho &= \sum_{m=0}^{\infty} \rho_m \ , \\ \vec{j} &= \sum_{m=0}^{\infty} \vec{j_m} \ , \\ \rho_m &= \frac{I_m \delta(s-ct)\delta(r-a)\cos(m\theta)}{\pi a^{m+1}(1+\delta_{m0})} \ , \\ \vec{j_m} &= c\rho_m \hat{s} \ , \end{aligned} \tag{3}$$

where m is the multipole moment present, I_m is the mth moment of the beam, and $\delta_{m0} = 1$ if $m = 0$, 0 otherwise.

Figure 2 gives the layout of the beam pipe; an infinitesimally thin ring charge with charge density ρ, current density $\vec{j}$, radius a, and angular dependence $\cos(m\theta)$ propagates along the s-axis of the pipe at the speed of light. The beam pipe has conductivity $\sigma \approx 10^{17}$ s^{-1}, radius $b \approx 5$ cm, and thickness $t \approx 1$ mm. The electromagnetic field experienced by a test charge at a distance z behind the ring charge in CGS units is thus given by the equations

$$\begin{aligned} \frac{1}{r}\frac{\partial(rE_r)}{\partial r} + \frac{1}{r}\frac{\partial E_\theta}{\partial \theta} + \frac{\partial E_s}{\partial s} &= 4\pi\rho \ , \\ \frac{1}{r}\frac{\partial B_s}{\partial \theta} - \frac{\partial B_\theta}{\partial s} - \frac{1}{c}\frac{\partial E_r}{\partial t} &= \frac{4\pi}{c} j_r \ , \end{aligned}$$

$$\begin{aligned}
\frac{\partial B_r}{\partial s} - \frac{\partial B_s}{\partial r} - \frac{1}{c}\frac{\partial E_\theta}{\partial t} &= \frac{4\pi}{c} j_\theta \,, \\
\frac{1}{r}\frac{\partial (rB_\theta)}{\partial r} - \frac{1}{r}\frac{\partial B_r}{\partial \theta} - \frac{1}{c}\frac{\partial E_s}{\partial t} &= \frac{4\pi}{c} j_s \,, \\
\frac{1}{r}\frac{\partial (rB_r)}{\partial r} + \frac{1}{r}\frac{\partial B_\theta}{\partial \theta} + \frac{\partial B_s}{\partial s} &= 0 \,, \\
\frac{1}{r}\frac{\partial E_s}{\partial \theta} - \frac{\partial E_\theta}{\partial s} + \frac{1}{c}\frac{\partial B_r}{\partial t} &= 0 \,, \\
\frac{\partial E_r}{\partial s} - \frac{\partial E_s}{\partial r} + \frac{1}{c}\frac{\partial B_\theta}{\partial t} &= 0 \,, \\
\frac{1}{r}\frac{\partial (rE_\theta)}{\partial r} - \frac{1}{r}\frac{\partial E_r}{\partial \theta} + \frac{1}{c}\frac{\partial B_s}{\partial t} &= 0 \,.
\end{aligned} \tag{4}$$

In order to make the equations easier to solve, we write the electromagnetic field components in terms of their Fourier transforms,

$$\begin{aligned}
(E_s, E_r, B_\theta) &= \cos(m\theta) \int_{-\infty}^{\infty} \frac{dk}{2\pi} e^{ikz} (\tilde{E}_s, \tilde{E}_r, \tilde{B}_\theta), \\
(E_\theta, B_s, B_r) &= \sin(m\theta) \int_{-\infty}^{\infty} \frac{dk}{2\pi} e^{ikz} (\tilde{E}_\theta, \tilde{B}_s, \tilde{B}_r),
\end{aligned} \tag{5}$$

where the Fourier transformed components are functions of k and r and are complex quantities.

Solving for the case of the monopole moment $m = 0$, the field components $(E_\theta, B_s, B_r) = 0$. The Fourier transformed components can then be solved for the region inside the pipe $r < b$,

$$\begin{aligned}
\tilde{E}_s &= A(k), \\
\tilde{E}_r = \tilde{B}_\theta &= \begin{cases} -ikA\frac{r}{2} \,, & r < a, \\ -ikA\frac{r}{2} + \frac{2q}{r} \,, & a < r < b. \end{cases}
\end{aligned} \tag{6}$$

In order to determine the form of $A(k)$, we need to solve for the region inside the pipe walls $r > b$. Inside the metal walls,

$$\begin{aligned}
\rho &= 0, \\
\vec{j} &= \sigma \vec{E},
\end{aligned} \tag{7}$$

where the conductivity σ is assumed to be independent of k.

We now consider the cases where the pipe walls are infinitely thick, and where the pipe walls have some finite thickness t.

2.2 Infinite Pipe Wall Thickness

If the pipe walls are infinitely thick, we can solve for the fields inside the pipe walls using equations (4) and (7), as well as the conditions that $(\tilde{E}_s, \tilde{B}_\theta)$ are continuous at $r = b$, and that $(\tilde{E}_s, \tilde{B}_\theta) \to 0$ as $r \to \infty$. This gives the solution

$$\begin{aligned}
A(k) &= \frac{2q}{b}\left(\frac{ikb}{2} - \frac{\lambda}{k}\right)^{-1} \,, \\
\lambda(k) &= i\sqrt{-i\frac{4\pi\sigma k}{c}} \,,
\end{aligned} \tag{8}$$

where a term $-\frac{k}{\lambda}$ has been dropped since $\frac{k}{\lambda}$ is much smaller than $\frac{\lambda}{k}$ or $\frac{ikb}{2}$.

The field component E_s can now be determined by performing the inverse Fourier transform on $A(k)$,

$$E_s = \int_{-\infty}^{\infty} \frac{dk}{2\pi} e^{ikz} A(k) \,. \tag{9}$$

In order to calculate this integral, we need to find the location of the poles and branch cuts of $A(k)$ [3]. It can be shown that the poles of $A(k)$ are located at

$$k_p = \alpha^{\frac{2}{3}}(\pm\sqrt{3} - i) \,, \tag{10}$$

where α is a constant given by

$$\alpha = \frac{1}{b}\sqrt{\frac{2\pi\sigma}{c}} \approx 10^6 \text{ m}^{-\frac{3}{2}} \,, \tag{11}$$

and that $A(k)$ has a branch cut along the negative imaginary axis from the origin to infinity.

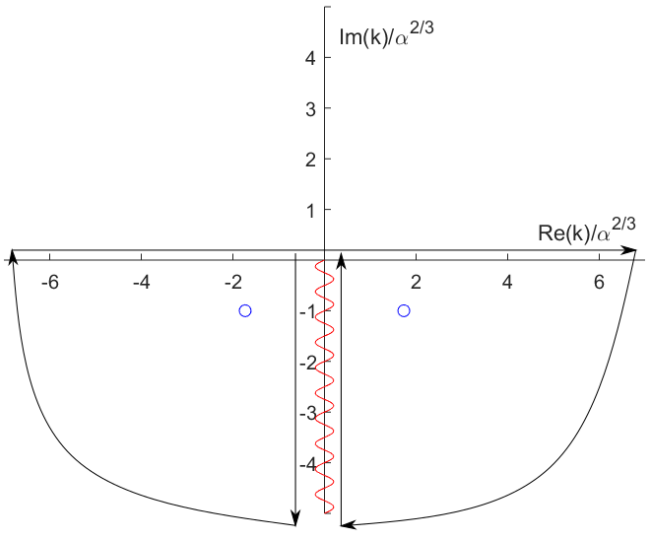

Figure 3: Plot of the integration contour and of the poles and branch cuts of $A(k)$

This allows us to calculate E_s in the infinite wall case,

$$\begin{aligned}
E_s &= -\frac{16q}{b^2}\left(\frac{1}{3}e^u \cos(\sqrt{3}u) - \frac{\sqrt{2}}{\pi}\int_0^\infty \frac{x^2 e^{ux^2}}{x^6 + 8} dx\right) \,, \\
u &= z\alpha^{\frac{2}{3}} \approx 10^4 z \,,
\end{aligned} \tag{12}$$

using values of $\sigma \approx 10^{17}$ s^{-1} and $b \approx 5$ cm. The full derivation of the location of the poles and branch cuts of $A(k)$ and of E_s can be found in Appendix A.

From Figure 4, we can see that E_s is proportional to $z^{\frac{3}{2}}$ at long ranges in the infinite wall case. We shall now investigate the long-range behaviour of E_s in the finite wall case.

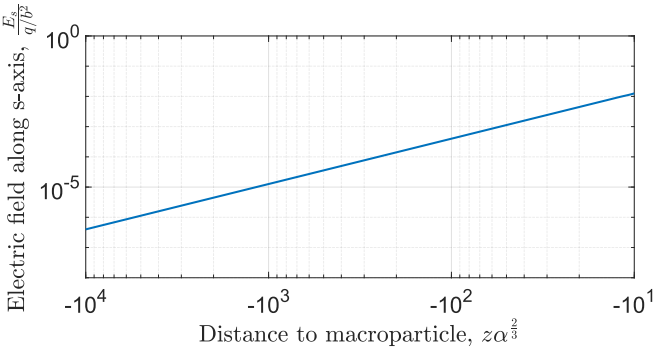

Figure 4: Long-range E_s for infinite pipe walls

2.3 Finite Pipe Wall Thickness

If the pipe walls have finite thickness t instead, the boundary conditions are similar to those in Section 2.2, except that $(\tilde{E}_s, \tilde{B}_\theta) = 0$ at $r = b + t$, instead of at $r \to \infty$. This leads to a different expression for $A(k)$,

$$\begin{aligned} A(k) &= \frac{2q}{b}\left(\frac{ikb}{2} - \frac{\lambda}{k}\frac{1+e^{2i\lambda t}}{1-e^{2i\lambda t}}\right)^{-1}, \\ &= \frac{2q}{b^2\alpha^{\frac{2}{3}}}\left(\frac{ik}{k_0} + \frac{k_0}{ik}\sqrt{-\frac{ik}{k_0}}\coth\left(\sqrt{-\frac{ik}{k_1}}\right)\right)^{-1}, \end{aligned} \tag{13}$$

where k_0 and k_1 are constants given by

$$\begin{aligned} k_0 &= 2\alpha^{\frac{2}{3}} = 2\left(\frac{2\pi\sigma}{cb^2}\right)^{\frac{1}{3}} \approx 2\times 10^4 \text{ m}^{-1}, \\ k_1 &= \frac{1}{2(b\alpha t)^2} = \frac{1}{2t^2}\frac{c}{2\pi\sigma} \approx 2\times 10^{-4} \text{ m}^{-1}, \end{aligned} \tag{14}$$

using a wall thickness of $t \approx 1$ mm and the same values of σ and b as in the infinite wall case.

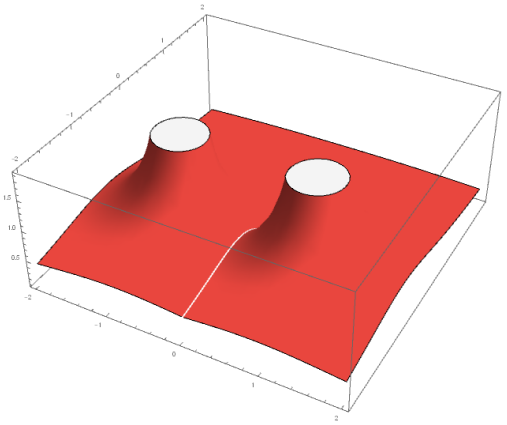

(a) $k_1 \to 0$

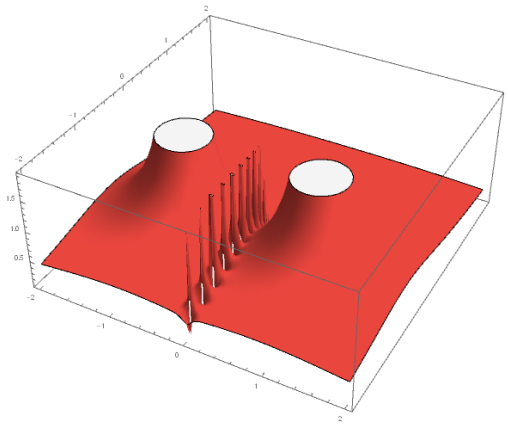

(b) $k_1 = 0.001$

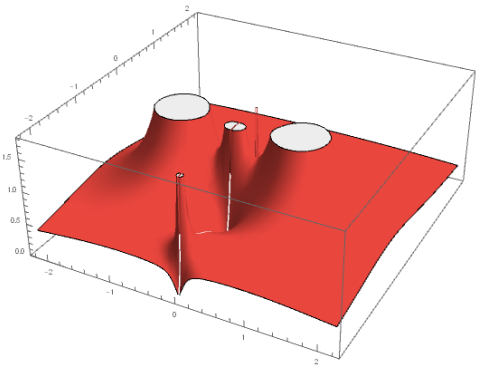

(c) $k_1 = 0.025$

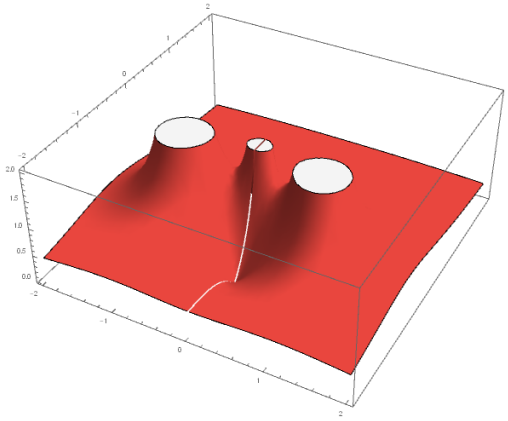

(d) $k_1 = 0.1$

Figure 5: 3D contour plots of poles of $A(k)$ for different values of k_1

3D contour plots of $A(k)$ for different values of k_1 (after setting $k_0 = 1\text{m}^{-1}$) are included in Figures 5(a) to (d).

Figure 5(a) shows that the infinite wall case ($k_1 \to 0$) has only 2 poles in the negative imaginary half-plane as well as a branch cut along the negative imaginary axis.

As k_1 increases to 0.001 in Figure 5(b), poles start to form along the negative imaginary axis. These poles spread further apart as k_1 increases further, in Figures 5(c) and (d).

From Equation 14, $k_1 \approx 10^{-8}\ k_0$, which implies that a very large number of poles along the negative imaginary axis are very closely spaced together, similar to the $k_1 = 0.001$ case.

In order to determine an analytic form of E_s for the finite wall case, we need to find the poles and branch cuts of $A(k)$. To determine if branch cuts are present, we can expand the coth term in Equation 13 about zero,

$$\begin{aligned}&\frac{ik}{k_0} + \frac{k_0}{ik}\sqrt{-\frac{ik}{k_0}}\coth\left(\sqrt{-\frac{ik}{k_1}}\right)\\ &\approx \frac{ik}{k_0} + \frac{k_0}{ik}\sqrt{-\frac{ik}{k_0}}\left(\left(\sqrt{-\frac{k_1}{ik}}\right) + \frac{1}{3}\left(\sqrt{-\frac{ik}{k_1}}\right) - ...\right).\end{aligned} \tag{15}$$

Since there are no fractional powers of k present in the denominator, $A(k)$ does not have a branch cut in the finite wall case. This is fundamentally different from the infinite wall case, where a branch cut extends along the negative imaginary axis. As a result, we expect to see a different analytic form for E_s in the finite thickness wall case.

The locations of the poles along the negative imaginary axis are determined by making the substitution

$$k = -ix^2 k_0 \tag{16}$$

into $A(k)$, where x is a real number, so that $A(x)$ is given by

$$A(x) = \frac{2q}{b^2\alpha^{\frac{2}{3}}}\left(x^2 + \frac{1}{x}\cot(px)\right)^{-1}, \tag{17}$$

where p is a constant given by

$$p = \sqrt{\frac{k_0}{k_1}}\,. \tag{18}$$

Using the values of k_0 and k_1 from Equation 14, $p \approx 10^4 >> 1$. Poles of $A(x)$ occur when the denominator is equal to 0, corresponding to solutions of the equation

$$\begin{aligned}&x^3 + \cot(px) = 0\,,\\ \implies\ &x^3 = -\cot(px)\,,\\ \implies\ &x^{-3} = -\tan(px)\,.\end{aligned} \tag{19}$$

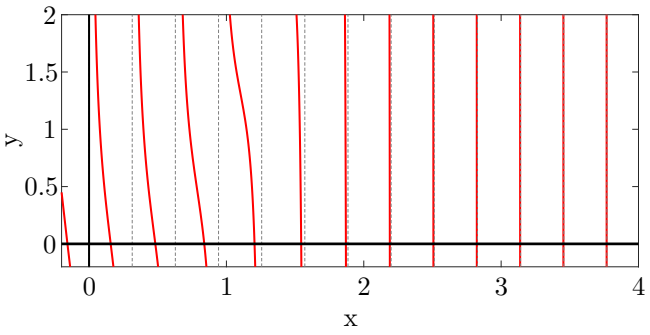

Figure 6: Plot of $y = x^3 + \cot(px)$ for $p = 10$

In the limit where $x \to 0$,

$$\cot(px) \approx 0\,,\ \implies x \approx \frac{(n-\frac{1}{2})\pi}{p}\ (\text{n integer})\,, \tag{20}$$

while in the opposite limit $x \to \infty$,

$$\tan(px) \approx 0\,,\ \implies x \approx \frac{n\pi}{p}\ (\text{n integer})\,. \tag{21}$$

Using these limits, we can say that the poles of $A(x)$ are located at

$$x_{p_n} = \frac{(n + f(n))\pi}{p}\,, \tag{22}$$

where $f(n)$ varies from $f(n) = -\frac{1}{2}$ at $n = 1$ to $f(n) = 0$ as $n \to \infty$.

In terms of $k = -ix^2 k_0$,

$$k_{p_n} = -i\left(\frac{(n + f(n))\pi}{p}\right)^2 k_0\,. \tag{23}$$

This makes finding the analytic form of E_s much simpler; instead of needing to integrate along a branch cut as in the infinite wall case, we can use Cauchy's Residue theorem at each pole of $A(k)$ to determine the complex integral.

We can write $A(x)$ as

$$A(x) = \frac{2qx}{b^2\alpha^{\frac{2}{3}}(x^3 + \cot(px))} = \frac{g(x)}{h(x)}\,, \tag{24}$$

where $g(x)$ and $h(x)$ are

$$\begin{aligned}g(x) &= \frac{2qx}{b^2\alpha^{\frac{2}{3}}}\,,\\ h(x) &= x^3 + \cot(px)\,.\end{aligned} \tag{25}$$

Thus, the residue of $A(k)$ at $k = k_{p_n}$ is

$$\begin{aligned}\mathrm{Res}(A(k),k_{p_n}) &= \frac{g(k_{p_n})}{\frac{dh}{dk}|_{k=k_{p_n}}} ,\\ &= \frac{g(k_{p_n})}{\frac{dh}{dx}|_{x=x_{p_n}}\frac{dx}{dk}|_{x=x_{p_n}}} ,\\ &= \frac{g(x_{p_n})}{h'(x_{p_n})}\frac{dk}{dx}\Big|_{x=x_{p_n}} .\end{aligned} \tag{26}$$

Evaluating the expressions for $g(x)$ and $h(x)$ at $x = x_{p_n}$ gives

$$\begin{aligned}\mathrm{Res}(A(k),k_{p_n}) &= \frac{2qx_{p_n}(-2ik_0x_{p_n})}{b^2\alpha^{\frac{2}{3}}(3x_{p_n}^2 - p\csc^2(px_{p_n}))} ,\\ &= \frac{-4ik_0qx_{p_n}^2}{b^2\alpha^{\frac{2}{3}}(3x_{p_n}^2 - p(1+\cot^2(px_{p_n})))} ,\\ &= \frac{-4i(2\alpha^{\frac{2}{3}})qx_{p_n}^2}{b^2\alpha^{\frac{2}{3}}(3x_{p_n}^2 - p(1+x_{p_n}^6))} ,\\ &= \frac{-8iqx_{p_n}^2}{b^2(3x_{p_n}^2 - p(1+x_{p_n}^6))} .\end{aligned} \tag{27}$$

Using Cauchy's Residue theorem the contribution to E_s from the poles along the negative imaginary axis is

$$\begin{aligned}E_s &= -2\pi i\sum_{n=1}^{\infty}\mathrm{Res}(A(k),k_{p_n}) ,\\ &= \frac{8q}{b^2}\sum_{n=1}^{\infty}\frac{x_{p_n}^2e^{zk_0x_{p_n}^2}}{p(1+x_{p_n}^6)-3x_{p_n}^2} .\end{aligned} \tag{28}$$

Thus, including the contribution from the other two poles in the negative imaginary half-plane, the total electric field along the s-axis is given by

$$\begin{aligned}E_s \approx -\frac{16q}{b^2}\Bigg(&\frac{1}{3}e^u\cos\left(\sqrt{3}u\right) - ...\\ &-\frac{1}{2}\frac{8q}{b^2}\sum_{n=1}^{\infty}\frac{x_{p_n}^2e^{zk_0x_{p_n}^2}}{p(1+x_{p_n}^6)-3x_{p_n}^2}\Bigg) .\end{aligned} \tag{29}$$

Whilst the first term is the same as in the infinite wall case due to the poles at $k_p = \alpha^{\frac{2}{3}}(\pm\sqrt{3}-i)$ not moving, the branch cut integral has now been replaced by an infinite sum of the residues of $A(k)$ at every pole along the imaginary axis.

This makes it difficult to determine the long-range behaviour of E_s in the finite wall case, since we need to include every term in the sum to obtain an accurate analytic form of E_s.

For the case of $p = 1\times10^4$ (typical of most real-world examples), finding an approximate form of the sum is difficult since the poles are not evenly spaced. As a result, it is not possible to approximate the entire sum as an integral using the Midpoint Rule.

However, we can consider the case where p is a much smaller value, such as $p = 10$. Figure 6 shows that the poles of $A(x)$ become approximately evenly spaced after the first p poles, so we can approximate the sum by writing out the explicit form of the residue of the first few poles, then approximating the rest of the sum with the Midpoint Rule.

The first 10 solutions of $x^3 + \cot(px) = 0$ for $p = 10$ are located at

$$\begin{aligned}x_p \approx 0.1575, 0.4824, 0.8387, 1.2047, 1.5443,\\ 1.8698, 2.1896, 2.5069, 2.8230, 3.1384...\end{aligned} \tag{30}$$

Then, the 11^{th} pole and onwards are located at

$$\begin{aligned}x_{p_{11}} &\approx \frac{11\pi}{p} ,\\ x_{p_{12}} &\approx \frac{12\pi}{p} ,\\ x_{p_{13}} &\approx \frac{13\pi}{p} ,\end{aligned} \tag{31}$$

with a spacing

$$\Delta x \approx \frac{\pi}{p} . \tag{32}$$

Suppose we had intervals of width $\Delta x = \frac{\pi}{p}$ starting from $x = \frac{21\pi}{2p}, \frac{23\pi}{2p}, ...$, which give midpoints of $x = \frac{11\pi}{p}, \frac{12\pi}{p}, ...$ and so forth. We can write the sum as

$$\begin{aligned}\sum_{n=1}^{\infty}\frac{x_{p_n}^2e^{zk_0x_{p_n}^2}}{p(1+x_{p_n}^6)-3x_{p_n}^2} \approx &\sum_{n=1}^{10}\frac{x_{p_n}^2e^{zk_0x_{p_n}^2}}{p(1+x_{p_n}^6)-3x_{p_n}^2}\\ &+\int_{\frac{21\pi}{2p}}^{\infty}\frac{px_p^2e^{zk_0x_p^2}}{\pi(p(1+x_p^6)-3x_p^2)}dx_p .\end{aligned} \tag{33}$$

The electric field is then given by

$$\begin{aligned}E_s \approx -\frac{16q}{b^2}\Bigg(&\frac{1}{3}e^u\cos\left(\sqrt{3}u\right) - ...\\ &-\frac{1}{2}\sum_{n=1}^{10}\frac{x_{p_n}^2e^{zk_0x_{p_n}^2}}{p(1+x_{p_n}^6)-3x_{p_n}^2} - ...\\ &-\frac{1}{2}\int_{\frac{21\pi}{2p}}^{\infty}\frac{px_p^2e^{2ux_p^2}}{\pi(p(1+x_p^6)-3x_p^2)}dx_p\Bigg) .\end{aligned} \tag{34}$$

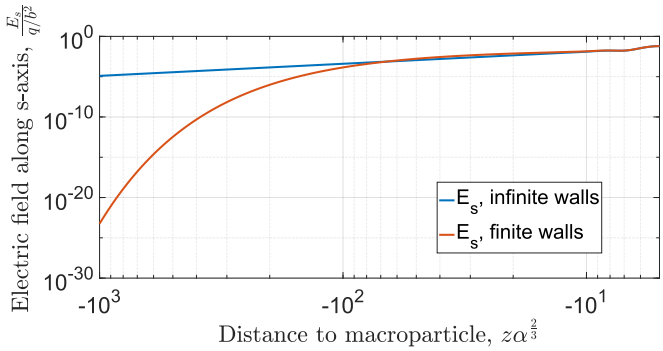

Figure 7: Long-range electric field in both the infinite and finite wall case for $p = 10$

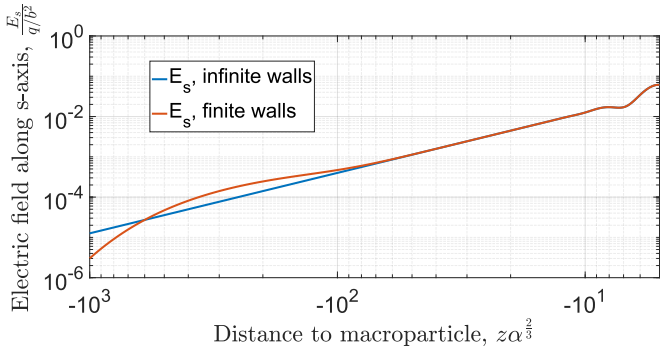

Figure 8: Long-range electric field in both the infinite and finite wall case for $p = 30$

Figure 7 shows that, in the finite thickness wall case, E_s transitions from obeying a $z^{\frac{3}{2}}$ power law relation to exponentially decaying as z becomes more negative. This is different from the infinite wall case, where it obeys a $z^{\frac{3}{2}}$ power law relation for all $z\alpha^{\frac{2}{3}} < -1$, which suggests that finite thickness walls reduce long-range wake effects experienced by charged particles, leading to greater beam stability.

Following the same procedure for $p = 30$, Figure 8 shows that the point where E_s transitions from obeying a power law to exponential decay occurs at a more negative z value than for $p = 10$. This suggests that E_s would begin to exponentially decay at large values of z for the case where $p = 10^4$, meaning that the long-range wake effects are significantly reduced compared to that of the infinite wall thickness case.

However, more work is required to determine the point where this transition occurs for large values of p, and to determine the accuracy of the integral approximation to the sum.

3 Impedance

Given that it is difficult to determine the long-range behaviour of the wake fields in terms of position, we can instead examine the Fourier transform of the wake fields, also known as the impedance, in order to determine their frequency response.

The longitudinal impedance $Z_m^{\parallel}(\omega)$ and the transverse impedance $Z_m^{\perp}(\omega)$ are related to $A(k)$ by

$$\frac{Z_m^{\parallel}(\omega)}{L} = \frac{\omega}{c}\frac{Z_m^{\perp}(\omega)}{L} = -\frac{1}{I_m c}A_m(k)\,, \tag{35}$$

where $\omega = ck$, $A_m(k)$ is the k-dependent coefficient of $\tilde{E}_s$ caused by the mth moment of the charge, and L is the length of the beam pipe section that contains the wake field.

$A_0(k)$ is given by Equations 8 and 13,

$$A_0(k) = \begin{cases} \frac{2q}{b}\left(\frac{ikb}{2} - \frac{\lambda}{k}\right)^{-1}, & \text{infinite wall,} \\ \frac{2q}{b}\left(\frac{ikb}{2} - \frac{\lambda}{k}\frac{1+e^{2i\lambda t}}{1-e^{2i\lambda t}}\right)^{-1}, & \text{finite wall .} \end{cases} \tag{36}$$

Solving Maxwell's equations for the $m \geq 1$ moments similarly gives expressions for $A_m(k)$ when $m \geq 1$,

$$A_m(k) = \begin{cases} \frac{4I_m}{b^{2m+1}}\left(\frac{ikb}{m+1} - \frac{\lambda}{k} - \frac{im}{kb}\right)^{-1}, \\ \frac{4I_m}{b^{2m+1}}\left(\frac{ikb}{m+1} - \frac{\lambda}{k}\frac{1+e^{2i\lambda t}}{1-e^{2i\lambda t}} - \frac{im}{kb}\right)^{-1}, \end{cases} \tag{37}$$

where the upper expression is for the infinite wall case and the lower expression is for the finite wall case.

In this example, we focus on the $m = 0$ longitudinal impedance and the $m = 1$ transverse impedance since they are the dominant terms for resistive wall effects. Solving for the relevant impedances gives

$$\frac{Z_0^{\parallel}(\omega)}{L} = \begin{cases} \frac{2}{bc}\left(\frac{\lambda c}{\omega} - \frac{i\omega b}{2c}\right)^{-1}, \\ \frac{2}{bc}\left(\frac{\lambda c}{\omega}\frac{1+e^{2i\lambda t}}{1-e^{2i\lambda t}} - \frac{i\omega b}{2c}\right)^{-1}, \end{cases} \tag{38}$$

$$\frac{Z_1^{\perp}(\omega)}{L} = \begin{cases} \frac{4}{\omega b^3}\left(\frac{\lambda c}{\omega} + \frac{ic}{\omega b} - \frac{i\omega b}{2c}\right)^{-1}, \\ \frac{4}{\omega b^3}\left(\frac{\lambda c}{\omega}\frac{1+e^{2i\lambda t}}{1-e^{2i\lambda t}} + \frac{ic}{\omega b} - \frac{i\omega b}{2c}\right)^{-1}, \end{cases} \tag{39}$$

where the upper expressions are for the infinite wall case, and the lower expressions are for the finite wall case.

3.1 Skin Depth

In order to get an idea of the frequency range at which long-range wake effects start to dominate, consider the frequency and skin depth to which the first pole of $A(k)$ corresponds.

The skin depth δ_s of a material is a measure of how far electromagnetic waves penetrate into the material before they are attenuated. δ_s is related to the quantity λ from Equation 8 by

$$\delta_s = \frac{1}{\mathrm{Im}(\lambda)} = \frac{c}{\sqrt{2\pi\sigma|\omega|}}\,, \tag{40}$$

which shows that materials have a larger skin depth for lower frequency waves.

For $\delta_s << t$, only a very small difference between the infinite and finite wall wake field is expected as the electromagnetic waves will be almost entirely attenuated by the time they have travelled a distance t through the wall.

However, when $\delta_s \approx t$, a large proportion of the initial electromagnetic wave will permeate through the finite pipe wall, potentially leading to decreased long-range wake effects.

Given a wall thickness of $t \approx 1$ mm, conductivity $\sigma \approx 10^{17}\text{s}^{-1}$, and pipe radius $b \approx 5$ cm as in Section 2, the frequency at which $\delta_s \approx t$ is given by

$$\omega \approx 1.4 \times 10^5 \text{ rad s}^{-1} . \tag{41}$$

Thus, if the first pole of $A(k)$ corresponds to a frequency of order 10^5 Hz, we expect the finite thickness of the pipe walls to have an effect on the long-range wake field.

From Equation 20, the first pole of $A(k)$ occurs at

$$x \approx \frac{\pi}{2p} , \tag{42}$$

where $p = 1 \times 10^4$ as is the case in most real-world situations. Using $k = -ix^2 k_0$ from Equation 16 and $|\omega| = c|k|$ gives

$$\omega \approx 1.5 \times 10^5 \text{ rad s}^{-1} . \tag{43}$$

This corresponds almost perfectly to the frequency at which skin depth effects become important, suggesting that wall thickness could have an effect on the long-range behaviour of the wake fields.

3.2 Longitudinal Impedance

Now that the frequency at which long-range wake effects start to dominate has been calculated, we can examine how wall thickness affects the longitudinal and transverse impedances.

Equation 38 shows that the low frequency behaviour of $Z_0^{\parallel}$ for a pipe with infinitely thick walls is proportional to $|\omega|^{\frac{1}{2}}$,

$$\frac{Z_0^{\parallel}(\omega)}{L} \approx \frac{1}{bc}\sqrt{\frac{|\omega|}{2\pi\sigma}}(1-i) . \tag{44}$$

Figures 9(a) to (d) shows that the low-frequency impedance obeys different power laws for the finite and infinite wall cases.

Figures 9(c) and 9(d) show that, at low frequencies, the finite wall impedance has a real and imaginary part proportional to $|\omega|^2$ and $-|\omega|$ respectively, in comparison to the infinite wall behaviour of $|\omega|^{\frac{1}{2}}$ and $-|\omega|^{\frac{1}{2}}$.

As the frequency increases beyond 10^5 Hz, the finite wall impedance tends towards the infinite wall impedance.

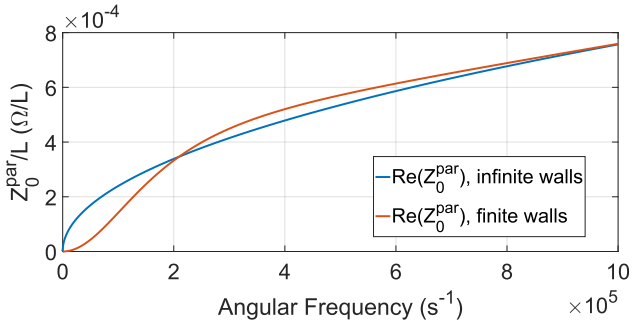

(a) Frequency response of the real part of the longitudinal impedance

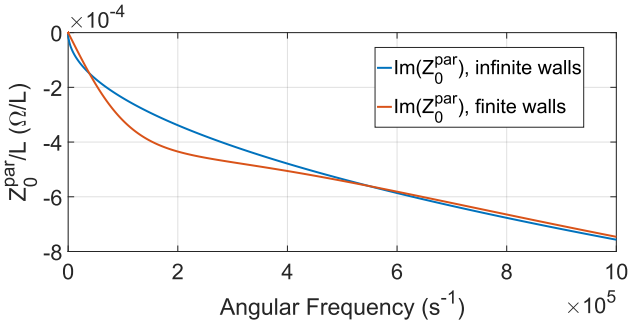

(b) Frequency response of the imaginary part of the longitudinal impedance

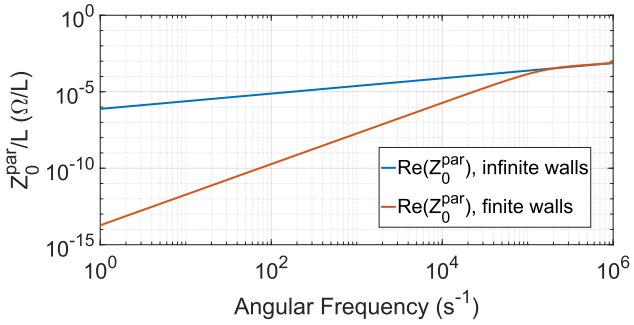

(c) Plot of the real part of the longitudinal impedance

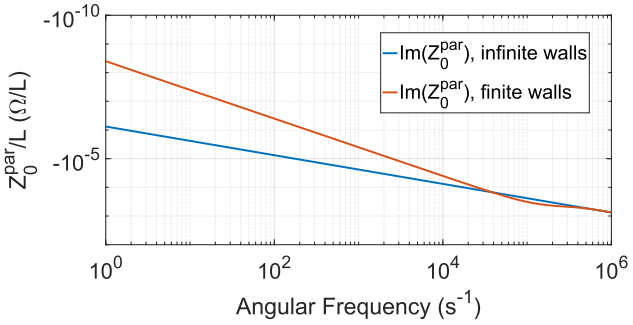

(d) Plot of the imaginary part of the longitudinal impedance

Figure 9: Plots of the real and imaginary parts of $Z_0^{\parallel}$

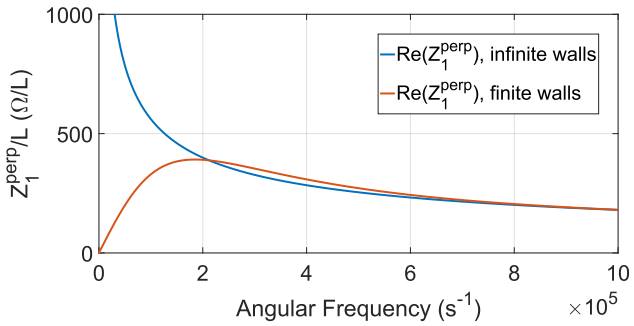

(a) Frequency response of the real part of the transverse impedance

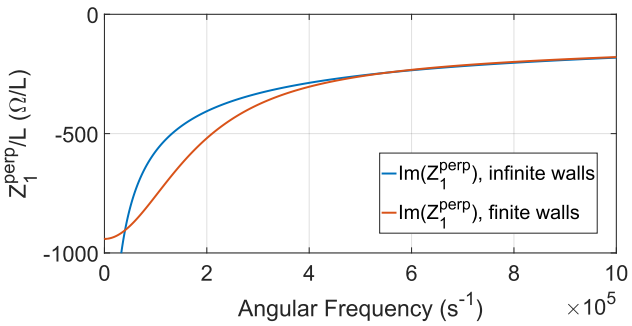

(b) Frequency response of the imaginary part of the transverse impedance

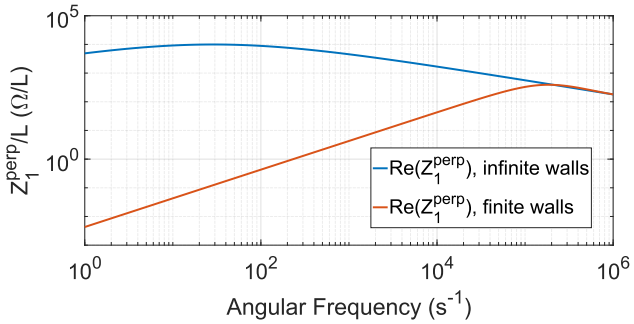

(c) Plot of the real part of the transverse impedance

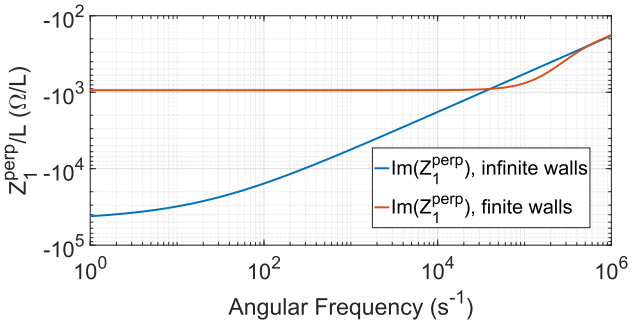

(d) Plot of the imaginary part of the transverse impedance

Figure 10: Plots of the real and imaginary parts of $Z_1^{\perp}$

This corresponds to the skin depth becoming much smaller than the wall thickness, so that the finite thickness pipe wall is essentially infinitely thick to electromagnetic radiation.

It can also be seen that, for frequencies $\omega \lesssim 10^4$ Hz, the total impedance is smaller in the finite wall case, leading to smaller long-range wake effects than in infinite pipe walls.

3.3 Transverse Impedance

In the case of the transverse impedance, Equation 39 can be used to show that the low frequency behaviour of $Z_1^{\perp}$ for a pipe with infinitely thick walls is proportional to $|\omega|^{-\frac{1}{2}}$,

$$\frac{Z_1^{\perp}(\omega)}{L} \approx \frac{1}{b^3}\sqrt{\frac{2}{\pi\sigma|\omega|}}(1-i)\,. \tag{45}$$

Figures 10(a) to (d) show that the finite wall case obeys different power laws to the infinite wall case at low frequencies, and that the finite wall case tends towards the infinite wall case as frequency increases, similar to the longitudinal impedance.

However, in this case, Figures 10(c) and 10(d) show that the finite wall impedance has a real part proportional to $|\omega|$ and a constant imaginary part, in comparison to the infinite wall behaviour of $|\omega|^{-\frac{1}{2}}$ and $-|\omega|^{-\frac{1}{2}}$ for the real and imaginary parts respectively.

Once again, the total impedance is smaller in the finite wall case for frequencies $\omega \lesssim 10^4$ Hz. Though further work is needed to obtain the relevant wake fields through inverse Fourier transforming the impedance expressions, we can see that the long-range, low-frequency wake is reduced when a beam pipe with a finite thickness of about 1 mm is used.

4 Conclusion

Using a beam pipe with finite thickness walls results in the long-range wake fields created by the monopole charge distribution decaying exponentially, as opposed to following a $|z|^{\frac{3}{2}}$ power law as in the infinite wall case. A similar procedure to that used in Section 2.1 could be used to determine the other field components for higher charge multipole moments.

For the $m = 0$ component of E_s, the Fourier transform of E_s in the finite wall case has no branch cut along the negative imaginary axis like in the infinite wall case, but instead has multiple poles along the negative imaginary axis. This allows Cauchy's Residue theorem to be used to obtain an analytic expression for E_s. Whilst this expression can be approximated for small values of p, further work is needed to determine a suitable way of approximating the infinite sum term for the large p values that typically occur in most linear accelerators.

The low-frequency longitudinal and transverse impedances of a beam pipe with finite thickness walls

also obey different power laws than for a beam pipe with infinitely thick walls. For frequencies less than about 10^4 Hz, both impedances for the finite wall case are smaller than for the infinite wall case, suggesting that the long-range wake field from the impedances is also reduced. This could be further investigated by examining the long-range behaviour of the wake field expressions that are obtained through Inverse Fourier transforming the impedance.

References

[1] A. W. Chao, *Physics of collective beam instabilities in high energy accelerators*. New York, NY: Wiley, 1993.

[2] S. Peggs and V. Mane, "KRAKEN, a numerical model of RHIC impedances," in *Proceedings Particle Accelerator Conference*, pp. 3137–3139, May 1995.

[3] K. L. F. Bane and M. L. Sands, "The Short-Range Resistive Wall Wakefields," June 1995.

A Solving E_s in the Infinite Wall Thickness Case

A.1 Finding Poles and Branch Cuts of $A(k)$

Inside the pipe region ($r < b$, where b is the radius of the inner region of the pipe),

$$\tilde{E_s} = A \,, \tag{46}$$

where

$$\begin{aligned} A &= \frac{2q}{b}\left(\frac{ikb}{2} - \frac{\lambda}{k}\right)^{-1} \,, \\ \lambda &= i\sqrt{-i\frac{4\pi\sigma k}{c}} \,. \end{aligned} \tag{47}$$

The function A has poles when its denominator is zero,

$$\begin{aligned} \frac{ikb}{2} - \frac{\lambda}{k} &= 0 \,, \\ \text{or} \frac{ikb}{2} - \frac{i}{k}\sqrt{-i\frac{4\pi\sigma k}{c}} &= 0 \,, \\ \implies ik &= -\frac{1}{ik}\frac{2}{b}\sqrt{-i\frac{4\pi\sigma k}{c}} \,, \\ \implies (-ik)^{\frac{3}{2}} &= -\frac{2}{b}\sqrt{\frac{4\pi\sigma}{c}} \,, \\ &= -2\sqrt{2}\alpha \,, \end{aligned} \tag{48}$$

where $\alpha = \frac{1}{b}\sqrt{\frac{2\pi\sigma}{c}}$. Solving for $(-ik)$,

$$\begin{aligned} (-ik)^3 &= 8\alpha^2 \,, \\ &= 8\alpha^2(e^0, e^{-i2\pi}, e^{i2\pi}) \,. \\ \implies (-ik) &= 2\alpha^{\frac{2}{3}}(e^0, e^{-i\frac{2\pi}{3}}, e^{i\frac{2\pi}{3}}) \,. \end{aligned} \tag{49}$$

However, for $(-ik) = 2\alpha^{\frac{2}{3}}$,

$$(-ik)^{\frac{3}{2}} + 2\sqrt{2}\alpha = 2\sqrt{2}\alpha + 2\sqrt{2}\alpha \neq 0 \,. \tag{50}$$

For $(-ik) = 2\alpha^{\frac{2}{3}}e^{\pm i\frac{2\pi}{3}}$,

$$(-ik)^{\frac{3}{2}} + 2\sqrt{2}\alpha = 2\sqrt{2}\alpha e^{\pm i\pi} + 2\sqrt{2}\alpha = 0 \,. \tag{51}$$

Thus, the two poles of A are located at

$$\begin{aligned} (-ik) &= 2\alpha^{\frac{2}{3}}e^{i\frac{2\pi}{3}} \,, \\ \implies k &= 2\alpha^{\frac{2}{3}}e^{-i\frac{5\pi}{6}} \,, \\ &= \alpha^{\frac{2}{3}}(-\sqrt{3} - i) \,, \end{aligned} \tag{52}$$

and

$$\begin{aligned} (-ik) &= 2\alpha^{\frac{2}{3}}e^{-i\frac{2\pi}{3}} \,. \\ \implies k &= 2\alpha^{\frac{2}{3}}e^{-i\frac{13\pi}{6}} \,, \\ &= \alpha^{\frac{2}{3}}(\sqrt{3} - i) \,, \end{aligned} \tag{53}$$

About the origin, replacing $(-ik)$ with $re^{i\theta}$

$$\begin{aligned} \frac{ikb}{2} + \frac{1}{ik}\sqrt{-i\frac{4\pi\sigma k}{c}} &= \frac{-bre^{i\theta}}{2} - \frac{1}{r}e^{-i\theta}\sqrt{\frac{4\pi\sigma}{c}re^{i\theta}} \,, \\ &= \frac{-bre^{i\theta}}{2} - \frac{1}{\sqrt{r}}e^{-i\frac{\theta}{2}}\sqrt{\frac{4\pi\sigma}{c}} \,, \\ &= \begin{cases} \frac{br}{2} + \frac{b\sqrt{2}\alpha i}{\sqrt{r}}, & \theta = \pi \,, \\ \frac{br}{2} - \frac{b\sqrt{2}\alpha i}{\sqrt{r}}, & \theta = -\pi \,. \end{cases} \end{aligned} \tag{54}$$

This implies that the values of A at $\theta = \pm\pi$ are different, which means that the origin is a branch point and the branch cut is along the negative imaginary axis.

A.2 Solving the Integral

The electric field $E_s(z)$ is obtained by performing the inverse Fourier transform of $A(k)$,

$$E_s = \int_{-\infty}^{\infty}\frac{dk}{2\pi}e^{ikz}\frac{2q}{b\left(\frac{ikb}{2} + \frac{1}{ik}\sqrt{\frac{4\pi\sigma}{c}(-ik)}\right)} \,. \tag{55}$$

Let $(-ik) = s$. The Laurent expansion of $\left(\frac{ikb}{2} - \frac{i}{k}\sqrt{-i\frac{4\pi\sigma k}{c}}\right)^{-1}$ about $s = 2\alpha^{\frac{2}{3}}e^{i\frac{2\pi}{3}} = s_+$,

$$\begin{aligned} \frac{1}{\frac{ikb}{2} + \frac{1}{ik}\sqrt{-i\frac{4\pi\sigma k}{c}}} &= \frac{-1}{\frac{sb}{2} + \frac{1}{s}\sqrt{\frac{4\pi\sigma s}{c}}} \,, \\ &= \frac{-1}{s^{-\frac{1}{2}}\left(\frac{b}{2}s^{\frac{3}{2}} + \sqrt{2}b\alpha\right)} \,, \\ &= \frac{-s^{\frac{1}{2}}}{\frac{b}{2}(s_+ + (s - s_+))^{\frac{3}{2}} + \sqrt{2}b\alpha} \,, \\ &\approx \frac{s^{\frac{1}{2}}}{\sqrt{2}b\alpha\left(1 + \frac{3(s-s_+)}{2s_+} + ... - 1\right)} \,, \\ &\approx \frac{2s^{\frac{1}{2}}s_+}{3\sqrt{2}b\alpha(-ik - s_+)} \,, \\ &= \frac{2s^{\frac{1}{2}}s_+ i}{3\sqrt{2}b\alpha(k - s_+ i)} \,. \end{aligned} \tag{56}$$

Thus, the residue at $k = \alpha^{\frac{2}{3}}(-\sqrt{3} - i)$ (i.e. at the point $s = s_+ = 2\alpha^{\frac{2}{3}}e^{i\frac{2\pi}{3}}$) is given by

$$\begin{aligned}\mathrm{Res}\Big(k=\alpha^{\frac{2}{3}}(-\sqrt{3}-i)\Big) &= \frac{2is_+^{\frac{3}{2}}}{3\sqrt{2}b\alpha}\ ,\\ &= \frac{2i(-2\sqrt{2}\alpha)}{3\sqrt{2}b\alpha}\ ,\\ &= \frac{-4i}{3b}\ .\end{aligned} \tag{57}$$

Similarly, the Laurent expansion about the point $s = 2\alpha^{\frac{2}{3}}e^{i\frac{-2\pi}{3}} = s_-$ is

$$\begin{aligned}&\frac{1}{\frac{ikb}{2}+\frac{1}{ik}\sqrt{-i\frac{4\pi\sigma k}{c}}} = \frac{2s^{\frac{1}{2}}s_-i}{3\sqrt{2}b\alpha(k-s_-i)}\ .\\ \implies &\mathrm{Res}\Big(k=\alpha^{\frac{2}{3}}(\sqrt{3}-i)\Big) = \frac{2is_-^{\frac{3}{2}}}{3\sqrt{2}b\alpha}\ ,\\ &= \frac{-4i}{3b}\ .\end{aligned} \tag{58}$$

Using Cauchy's residue theorem (since the integration contour is clockwise, the integral around one of the poles is $(-2\pi i)$ times the residue of that pole),

$$\begin{aligned}E_s &= -2\pi i\bigg(\frac{q}{b\pi}\Big(\frac{-4i}{3b}(e^{z\alpha^{\frac{2}{3}}(1-\sqrt{3})}+e^{z\alpha^{\frac{2}{3}}(1+\sqrt{3})})\Big)\bigg)\\ &\quad + [\text{Branch cut integral}]\ ,\\ &= -\frac{16q}{3b^2}e^u\cos\big(\sqrt{3}u\big) + [\text{Branch cut integral}]\ ,\end{aligned} \tag{59}$$

where $u = z\alpha^{\frac{2}{3}}$.

Transforming coordinates from k to r using $(-ik) = re^{\pm i\pi}$,

$$\begin{aligned}k &= ire^{\pm i\pi}\\ \implies dk &= ie^{\pm i\pi}dr\ .\end{aligned} \tag{60}$$

Performing the branch cut integral and substituting k,

$$\begin{aligned}I &= \int_{-\infty}^{0}\frac{ie^{i\pi}}{2\pi}e^{-zre^{i\pi}}\frac{2q}{b\Big(\frac{b}{2}\Big(r+\frac{2\sqrt{2}}{\sqrt{r}}\alpha i\Big)\Big)}dr\\ &\quad+\int_0^{\infty}\frac{ie^{-i\pi}dr}{2\pi}e^{-zre^{-i\pi}}\frac{2q}{b\Big(\frac{b}{2}\Big(r-\frac{2\sqrt{2}}{\sqrt{r}}\alpha i\Big)\Big)}dr\ ,\\ &= -\frac{2q}{b^2\pi}\bigg(-\int_0^{\infty}ie^{zr}\frac{r-\frac{2\sqrt{2}}{\sqrt{r}}\alpha i}{r^2+\frac{8\alpha^2}{r}}dr\\ &\qquad+\int_0^{\infty}ie^{zr}\frac{r+\frac{2\sqrt{2}}{\sqrt{r}}\alpha i}{r^2+\frac{8\alpha^2}{r}}dr\bigg)\ ,\\ &= -\frac{8\sqrt{2}q}{b^2\pi}\bigg(\int_0^{\infty}e^{zr}\frac{\alpha i^2}{r^{\frac{5}{2}}+\frac{8\alpha^2}{\sqrt{r}}}dr\bigg)\ .\end{aligned} \tag{61}$$

Using the substitution $r = x^2\alpha^{\frac{2}{3}} \implies dr = 2x\alpha^{\frac{2}{3}}dx$,

$$\begin{aligned}I &= \frac{8\sqrt{2}q}{b^2\pi}\bigg(\int_0^{\infty}e^{x^2z\alpha^{\frac{2}{3}}}\frac{\alpha}{x^5\alpha^{\frac{5}{3}}+\frac{8\alpha^2}{x\alpha^{\frac{1}{3}}}}2x\alpha^{\frac{2}{3}}dx\bigg)\ ,\\ &= \frac{16\sqrt{2}q}{b^2\pi}\bigg(\int_0^{\infty}\frac{x^2e^{ux^2}}{x^6+8}dx\bigg)\ ,\end{aligned} \tag{62}$$

where $u = z\alpha^{\frac{2}{3}}$ as before. Thus, E_s is given by

$$E_s = -\frac{16q}{b^2}\bigg(\frac{1}{3}e^u\cos\big(\sqrt{3}u\big) - \frac{\sqrt{2}}{\pi}\int_0^{\infty}\frac{x^2e^{ux^2}}{x^6+8}dx\bigg)\ . \tag{63}$$

Equation 63 gives the behaviour of E_s at both small and large $|z|$.